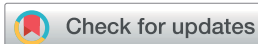


PAPER



Cite this: *J. Mater. Chem. A*, 2017, 5, 15183

Oxygen activity and peroxide formation as charge compensation mechanisms in Li_2MnO_3

Anika Maruszczyk,^{*ab} Jan-Michael Albina,^a Thomas Hammerschmidt,^a Ralf Drautz,^a Thomas Eckl^b and Graeme Henkelman^b 

In the search for high energy density battery materials, over-lithiated transition metal oxides have attracted the attention of many researchers worldwide. There is, however, no consensus regarding the underlying mechanisms that give rise to the large capacities and also cause the electrochemical degradation upon cycling. As a key component and prototype phase, Li_2MnO_3 is investigated using density functional theory. Our calculations show that hole doping into the oxygen bands is the primary charge compensation mechanism in the first stage of delithiation. Upon further delithiation, there is an energetic driving force for peroxide formation with an optimal number of peroxide dimers that is predicted as a function of lithium concentration. Unlike the defect-free phases, the peroxide structures are highly stable, which leads to two competing mechanisms for charge compensation: (i) oxygen loss and densification at the surface and (ii) peroxide formation in the bulk. Our results show that both have a detrimental effect on the electrochemical performance and therefore the stabilization of oxygen in the crystal lattice is vital for the development of high energy cathode materials. The insights into the origin and implications of peroxide formation open the door for a more profound understanding of the degradation mechanism and how to counteract it.

Received 13th May 2017
Accepted 3rd July 2017

DOI: 10.1039/c7ta04164k

rsc.li/materials-a

1 Introduction

The goal of automobile electrification has motivated a search for battery materials that meet the necessary requirements. Crucial for the success of this effort is the development of cathode materials that can provide high energy densities, sufficient rate capabilities, good cyclability, and low cost. These demands can, in principle, be achieved with over-lithiated transition metal oxides. One of the most prominent candidates is high-energy Ni–Co–Mn (HE-NCM), a composite often written as $x\text{Li}_2\text{MnO}_3 \cdot (1-x)\text{LiMO}_2$, ($M = \text{Ni}, \text{Co}, \text{Mn}$). The commercial use of HE-NCM is, however, impeded by polarization losses as well as significant fade in voltage and capacity upon cycling.^{1–3} Understanding the underlying mechanisms that give rise to the high Li capacity in the first cycle, as well as the subsequent electrochemical degradation, is an important step towards improving the material for use in vehicles. While higher over-lithiation leads to a higher initial capacity, the problems of voltage fade and hysteresis also increase with the Li_2MnO_3 content.³ As the key component of HE-NCM, end member, and prototype over-lithiated transition metal oxide

cathode material, the electrochemical properties of Li_2MnO_3 need to be better understood.

In the pure Li_2MnO_3 phase, all of the manganese atoms are tetravalent. The inability of Mn to be further oxidized¹ provides no obvious charge compensation mechanism for the removal of Li^+ . The material does, however, exhibit electrochemical activity when cycled above 4.5 V.^{4,5} An activation mechanism involving irreversible oxygen loss and a phase transformation from $\text{Li}_2\text{MnO}_3 \rightarrow \text{Li}_2\text{O} + \text{MnO}_2$ has been reported.^{6–8} The electrochemical performance of Li_2MnO_3 strongly depends on the synthesis conditions and while first cycle capacities of over 400 mA h g^{-1} have been achieved,⁹ the cycling behavior is generally quite poor.² This poor cycling behavior has been attributed to the formation of spinel-like domains after activation.^{2,4,10}

If oxygen loss was the only mechanism of charge compensation, the observed high capacity of Li_2MnO_3 would imply a much greater loss of oxygen from the active material than is measured.² Recent work suggests an alternative explanation, that oxygen can participate reversibly in the redox process.^{3,11,12} Additionally, the formation of peroxo/superoxo-like species^{13,14} and oxygen dimers with short bond lengths¹⁵ in structurally related systems have been reported. Reversible oxygen activity has so far not been directly observed in HE-NCM, which may be because it is difficult to differentiate simultaneous oxygen loss and oxidation.¹⁶ Previous studies on Li_2MnO_3 report hole doping into the oxygen 2p bands upon delithiation^{17–20} while the formation of oxygen dimers has so far only been observed in

^aICAMS, Ruhr Universität Bochum, Germany. E-mail: Anika.Maruszczyk@de.bosch.com

^bRobert Bosch GmbH, Renningen, Germany

^cDepartment of Chemistry, The Institute for Computational Engineering and Sciences, The University of Texas at Austin, Austin, TX 78712-0165, USA. E-mail: henkelman@utexas.edu; Fax: +1 512 471 8696; Tel: +1 512 471 4170

highly disordered^{3,19} or fully delithiated phases.²⁰ Both of these are unlikely to develop in the material upon cycling. So far, the spontaneous formation of a dimer in an ordered phase could not be explained from a thermodynamic perspective²⁰ and further insights into the formation mechanism are needed. There have been theoretical studies²¹ focusing on the general conditions for oxygen oxidation and dimer formation while the intricacies and implications of the associated reaction mechanism need to be further investigated.

In this present study, the important partially delithiated Li_2MnO_3 phases are investigated and for the first time a thermodynamic driving force for the formation of oxygen dimers upon more than half delithiation is observed. While the corresponding peroxide structures are disordered at intermediate states of charge, they become symmetric and highly stable upon further delithiation. This leads to a thermodynamic driving force for a phase separation into a fully lithiated and highly delithiated phase. The newly found configurations are analyzed on a thermodynamic level and their detrimental effect on the electrochemical performance is discussed. In this context, the driving force for oxygen dimerization is quantified. In contrast to coherent Li_2MnO_3 , the peroxide phases exhibit an increased stability against oxygen loss. This work leads to a model of peroxide formation in the bulk and oxygen release and densification at the surface.

2 Methods

Our density functional theory (DFT) calculations have been performed using the Vienna *Ab initio* Simulation Package^{22–24} with the Perdew–Burke–Ernzerhof parametrization of the generalized gradient approximation^{25,26} to describe electronic exchange and correlation. The projector augmented-wave framework (PAW)^{27,28} was used to model the core electrons and their interactions with the valence electrons. We chose to include the Mn semi-core p electrons explicitly in our calculations. A convergence analysis showed that an energy cutoff of 500 eV for the plane wave basis set and a k -point density of 445 points per \AA^{-3} provided sufficient accuracy for our results. To properly describe the localized Mn d-states, the DFT+U method was employed with an effective U value of 4.7 eV, which has been found to reproduce experimentally observed lithiation voltages in Li_2MnO_3 .^{17,29,30} All structures were fully relaxed in a spin-polarized calculation with high precision until the energy was converged to within 10^{-5} eV. Oxidation states in the materials were estimated from Bader charges³¹ and magnetic moments. For selected structures, additional calculations have been performed using the Heyd–Scuseria–Ernzerhof (HSE06)³² hybrid functionals that are understood to give a more reliable description of the oxygen binding energy and redox activity.²⁰ A mixing parameter of 0.17 was used, following ref. 21.

Li_2MnO_3 was modeled with a 48 atom supercell including eight formula units (FUs). To explore the most stable phases as a function of lithium concentration, the basin hopping algorithm was used,^{33,34} as implemented in the atomistic simulation environment.³⁵ Unless stated otherwise, all atoms were displaced at each basin hopping step. The efficiency of these

sampling calculations was increased by lowering the plane wave cutoff to 325 eV and by using softer PAW pseudopotentials. The most stable configurations were fully relaxed with the more accurate simulation parameters to obtain comparable energies. Images of the crystal structures have been produced using the Visualization for Electronic and Structural Analysis software.³⁶

3 Results and discussion

3.1 Li_2MnO_3 at low delithiation

Li_2MnO_3 is characterized by layers of octahedrally coordinated cations in a face centered cubic (FCC) oxygen lattice. The honeycomb ordering of the excess lithium in the transition metal layers has the monoclinic $C2/m$ symmetry. The fully lithiated structure, shown in Fig. 1, has charges and magnetic moments (Table 1) that are consistent with those previously found³⁷ for the covalently bound Mn^{4+} and O^{2-} . In agreement with previous experimental² and theoretical studies,^{17–19} Mn does not take part in the redox process and the charge upon Li removal is compensated through the introduction of holes into the oxygen 2p bands instead. This is illustrated by the density of states (Fig. 2), exhibiting oxygen bands near the Fermi level and hole creation upon delithiation. Additionally, the oxygen atoms acquire less negative charges and a magnetic moment, which has been reported as a signature of hole doping.^{19,20,38}

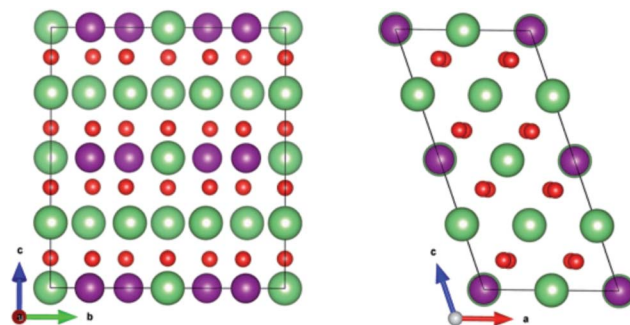


Fig. 1 Crystal structure of the fully lithiated Li_2MnO_3 phase in the bc - and ac -plane; green is Li; purple is Mn; red is O.

Table 1 Average oxidation states e for manganese and oxygen along with their average magnetic moments μ

x in Li_xMnO_3	Mn e	Mn μ	O e	O μ
2, coherent	+1.83	3.23	−1.18	−0.08
1.625, coherent	+1.83	3.24	−1.08	−0.19
1.25, coherent	+1.83	3.21	−0.97	−0.29
1, coherent	+1.84	3.23	−0.90	−0.36
0.25, coherent	+1.85	3.26	−0.69	−0.59
0.5, coherent	+1.84	3.30	−0.76	−0.53
0.5, peroxide	+1.72	3.88	−0.71	−0.29
0.25, peroxide	+1.60	4.41	−0.60	−0.09
LiMnO_2	+1.68	3.93	−1.28	−0.01

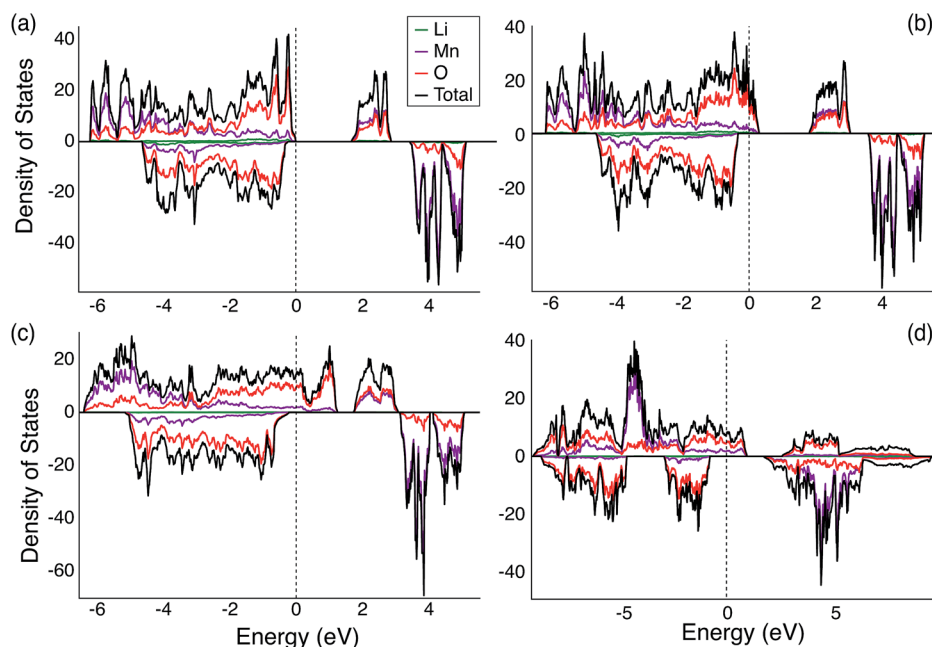


Fig. 2 Density of states of the (a) fully lithiated; (b) 18.75% delithiated; (c) 87.5% delithiated with a coherent O lattice; and (d) 87.5% delithiated peroxide structure.

3.2 Peroxide formation in $\text{Li}_{2-x}\text{MnO}_3$

As long as Li_2MnO_3 remains more than half lithiated, the crystal and atomic structure are stable. Upon higher states of charge, the most stable configurations exhibit pronounced lattice distortions accompanied by the formation of oxygen dimers with O–O bond lengths less than 1.6 Å. Since there is a distinct difference between the short peroxide bond lengths and those of the original lattice oxygen of more than 2 Å, this value has been chosen as a bond length cutoff for peroxide species. The oxygen dimers form in the layers with Li vacancies; these oxygen atoms have reduced Bader charges compared to the structural O^{2-} atoms. Upon formation of oxygen dimers, the oxygen magnetic moment drops close to zero (Table 1), indicating the formation of O_2^{2-} peroxide as a result of hole doping in the O_2^{3-} lattice.³⁹ The change in the oxygen peroxide bonding, as compared to the coherent oxygen lattice, is illustrated by the charge redistribution in Fig. 3; differences in the

O–Mn covalency are apparent. The change in electronic structure is reflected in the density of states in Fig. 2(d).

Based on our charge and magnetic moment analysis, Mn reduces its oxidation state in the presence of peroxides as a result of anionic charge over-compensation. This is in agreement with the Mn^{3+} fraction reported in partially relithiated HENCM.⁴⁰ The creation of Mn^{3+} species can have significant consequences for the material's performance. These include a low redox potential^{41,42} and a driving force for disproportionation and ion migration⁴³ that could lead to detrimental phase transformations.

To investigate the phase stability of Li_xMnO_3 , formation energies have been calculated as¹⁸

$$\Delta E = E(\text{Li}_x\text{MnO}_3) - (x/2) \cdot E(\text{Li}_2\text{MnO}_3) - (1 - x/2) \cdot E(\text{MnO}_3) \quad (1)$$

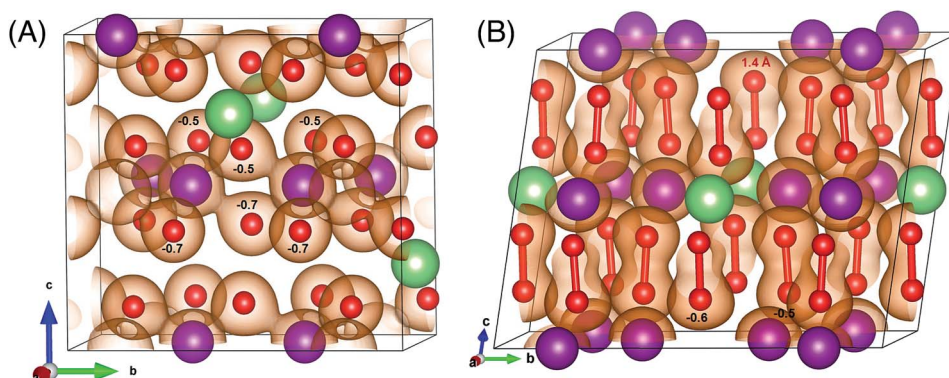


Fig. 3 Lowest energy $\text{Li}_{0.25}\text{MnO}_3$ structure with a (A) coherent oxygen lattice, and (B) peroxide lattice; red: O–O bond length; black: O oxidation state.

where E is the ground state energy of the annotated structures (Fig. 4). The blue points were obtained from Li_xMnO_3 configurations with a coherent oxygen lattice, while the red points correspond to peroxide phases. The latter exhibit lower formation energies and predict a phase separation into a fully lithiated and a highly delithiated phase (Fig. 3(B)). Intermediate $x > 0.25$ structures are unstable, which is especially pronounced for the coherent phases. It should be noted that the coherent oxygen lattice MnO_3 phase has been used as the fully delithiated end point. A more stable yet distorted end point configuration containing peroxide species leads to qualitatively similar results. The stability of the peroxide phases confirms the reported driving force for dimerization upon sufficient hole doping.^{20,44,45}

The corresponding peroxide configurations have, to the best of our knowledge, not been reported in previous computational studies. This may be due to the use of smaller cells,¹⁷ the consideration of higher lithium concentrations¹⁸ or the use of local rather than global structural optimization methods.²⁰ To confirm the stability of the structure shown in Fig. 3(B), we did a basin hopping global optimization calculation to search through phase space and did not find any lower energy phase in a search of 200 candidates. Similar investigations for delithiated structures with $x \leq 1$ generally resulted in highly disordered low-energy phases, in agreement with previous findings.^{3,19} These calculations provide evidence for the instability of Li_xMnO_3 structures with a coherent O-lattice at high states of charge that give rise to a driving force for peroxide formation. For further validation, selected structures have been investigated using hybrid functionals. Even though the energy difference between the most stable coherent and peroxide $\text{Li}_{0.25}\text{MnO}_3$ phase is not as pronounced as with GGA+U, the hybrid functional gives an energy of the latter that is lower by 229 meV per FU, confirming the stability of the peroxide phase.

The formation of peroxide phases is associated with strong geometrical changes and its occurrence might be kinetically impeded at common charging rates. Depending on the impact of these limitations, three different scenarios can be distinguished: Li_2MnO_3 either (i) experiences a phase separation into Li_2MnO_3 and peroxide $\text{Li}_{0.25}\text{MnO}_3$, (ii) retains a coherent oxygen lattice at all lithium concentrations or (iii) retains a coherent oxygen lattice upon initial delithiation and forms peroxides at

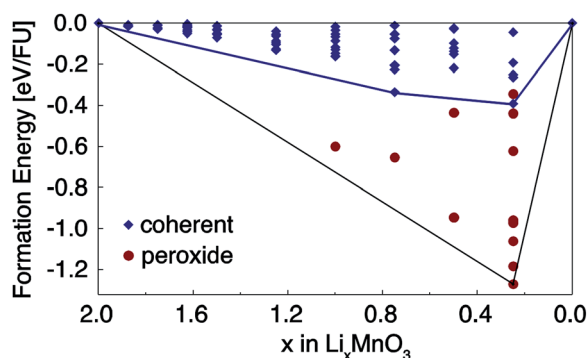


Fig. 4 Convex hull of stability for Li_xMnO_3 .

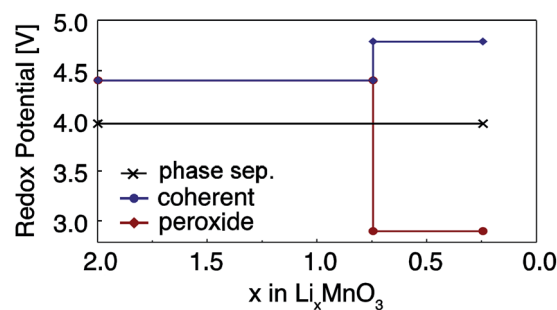


Fig. 5 Average redox potential of the structures with a coherent oxygen lattice and those in which the oxygen has formed peroxide species.

high states of charge. The corresponding redox potentials based on the associated phase stabilities (Fig. 4) are shown in Fig. 5. The phase separation leads to a voltage plateau at 3.97 V, which is notably lower than the experimentally observed 4.5 V value. Within the first cycles, neither Li_2MnO_3 (ref. 4) nor HE-NCM⁴⁶ exhibit significant electrochemical activity in this voltage region and the phase separation is therefore not expected to reversibly take place throughout the particle.

The voltage plateau associated with coherent delithiation is in better agreement with the experimentally observed first charge value.⁴ Since the pronounced electrochemical activity around 4.5 V is not observed upon subsequent discharge, the second model can also be excluded as a reversible process throughout the material. Based on the current results, Li_2MnO_3 must therefore predominantly remain coherent upon initial delithiation while the charge is compensated *via* hole creation in the oxygen bands at around 4.5 V. According to the third model, the unstable structure then transforms to a peroxide phase that is redox active at notably lower voltages and might therefore be reduced at higher states of charge than its formation. While there are several ways in which the transformation from coherent to peroxide Li_xMnO_3 might take place, the voltage associated with the formation of the most stable $\text{Li}_{0.25}\text{MnO}_3$ peroxide phase from coherent $\text{Li}_{0.75}\text{MnO}_3$ has been included in Fig. 5. To gain a more thorough understanding of the associated processes and their effect on the electrochemistry, the lithium concentration dependent reaction mechanism should be investigated in future work. There might be additional structural changes resulting from the peroxide phase formation that will be discussed in a future publication. As neither Li_2MnO_3 (ref. 2) nor HE-NCM³ exhibit long-range formation of a new ordered phase, the peroxide domains might only develop on a local scale. Since oxygen dimer formation is assumed to predominantly occur in the bulk, surface sensitive methods that would be able to detect the local change in bond length, such as Raman spectroscopy, might be inappropriate. This renders the experimental verification extremely challenging.

3.3 Relithiation of Li_xMnO_3

Unless further structural transformations take place, the coherent Li_2MnO_3 phase should be recovered from the peroxide

structures upon full relithiation. To identify the Li concentration at which dimers become unstable, the highly delithiated coherent oxygen lattice, Fig. 3(A), and peroxide phases, Fig. 3(B), have been used as input geometries for basin hopping calculations at various Li concentrations. In order to avoid severe structural distortions in our basin hopping calculations of metastable configurations, only the lithium atoms were displaced in each basin hopping trial move; note that each structure was then fully relaxed.

Fig. 6 shows the energies of the most stable configurations as well as selected crystal structures. The peroxide phases (red line) are most stable at high states of charge while the symmetric peroxide lattice is retained upon relithiation to $\text{Li}_{0.75}\text{MnO}_3$. This Li concentration is the point at which the relithiated peroxide phases become unstable with respect to the coherent lattice (blue line). The dimers tend to form between the Mn layers at high states of charge, and as soon as the Li concentration is sufficiently high, there is neither the space nor a driving force for the peroxide lattice for charge compensation. Upon further lithiation, the material transforms back to the original Li_2MnO_3 geometry at $x > 1.25$. This means that the peroxides that formed at high delithiation may only transform back into a coherent oxygen lattice at higher lithium concentrations, which would explain the observed hysteresis in cycling experiments.

The most stable Li_xMnO_3 configurations do not always exhibit ordered lattices at all Li concentrations. Instead, the lowest energy intermediate configurations, which correspond to those obtained by basin hopping as described in Section 3.2, are disordered phases with a few peroxides. Overall, the lowest energy structures found in this work (black line) can be characterized by a coherent lattice until the material is half delithiated; then the formation of peroxides and a disordered structure at intermediate states of charge, and finally at $x \leq 0.5$, symmetric peroxide phases emerge. The metastable coherent lattice structures (blue line) exhibit an orthorhombic geometry at high states of charge that is retained until $x = 1$, when Li_xMnO_3 first becomes unstable.

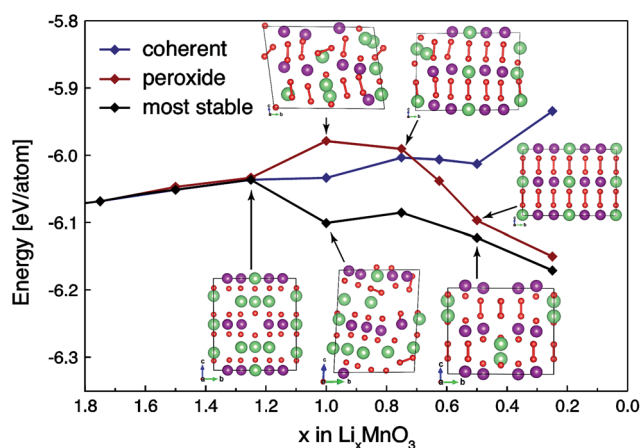


Fig. 6 Energy per atom vs. Li concentration upon relithiation of the coherent (blue) and peroxide (red) oxygen lattices, in comparison to the lowest energy structures found throughout this work (black) found primarily with basin hopping and by construction.

3.4 Peroxide formation and material stability

The formation of oxygen dimers increases the stability of Li_xMnO_3 at high delithiation, $x \leq 1$, while the peroxide structures are unstable at low states of charge. At the same time, the configurations containing the highest peroxide concentration are not always the most stable. The change in total energy per peroxide dimer must therefore depend both on the Li concentration, x , as well as the concentration of peroxides already present in the structure, c_{peroxide} . To describe this relation, a simple model has been developed that expresses the formation energies, defined as $E_{\text{model}} = E(\text{Li}_x\text{MnO}_3) - E(\text{MnO}_3) - xE(\text{Li})$, as a function of both Li and peroxide concentration,

$$E_{\text{model}} = xE_{\text{lith}} + c_{\text{peroxide}}(E_{\text{peroxide}} + \alpha x + \beta c_{\text{peroxide}}), \quad (2)$$

where E_{lith} is the energy associated with adding Li and therefore corresponds to the voltage. E_{peroxide} is the change in energy caused by the formation of an O-dimer and the parameters α and β account for the dependence of the peroxide formation energy on the lithium concentration, x , and the peroxide concentration c_{peroxide} . In order to obtain the unknown values, a data set of 119 calculated formation energies at various Li concentrations was used to fit this model. Peroxide species were identified as an atomic oxygen pair with a bond length less or equal to 1.6 Å. The fit gives parameters $E_{\text{lith}} = -4.56 \pm 0.02$, $E_{\text{peroxide}} = -2.67 \pm 0.44$, $\alpha = 1.67 \pm 0.24$ and $\beta = 1.31 \pm 0.27$.

The energy for the intercalation of Li, E_{lith} , coincides well with the voltage plateau at 4.5 V. From eqn (2), there are three competing terms determining whether the formation of peroxides is associated with an increase or decrease in energy. Generally speaking, the total energy only decreases by the formation of a dimer if the lithium concentration is sufficiently low and the optimal peroxide concentration has not been exceeded. By differentiation, this optimum is determined as $c_{\text{peroxide}}^{\text{opt}} = -0.63x + 1.02$.

For further validation of eqn (2), the peroxide concentrations in the most stable configurations among the 119 structures have been plotted against the lithium concentration in comparison to $c_{\text{peroxide}}^{\text{opt}}$ (Fig. 7). Clearly there is no driving force for peroxide formation at more than half lithiation; a linear dependence emerges at higher states of charge that coincides well with our simple model. The slope is intuitively close to one, demonstrating that a dimer is formed when a lithium atom is removed. At $x = 0.25$, two stable configurations with almost coinciding energies and peroxide concentrations of 0.58 and 1 have been included in the plot. Even though the model predicts an optimum concentration of 0.8 at this state of charge, a symmetric peroxide lattice with $c_{\text{peroxide}} = 1$ may be more favorable (Fig. 3(B)). Overall, the model illustrates the driving force for peroxide formation upon delithiation and the existence of an optimal number of dimers above which further peroxide formation requires energy at the corresponding lithium concentration.

3.5 Oxygen loss in Li_xMnO_3

Previous investigations have considered the stability of Li_xMnO_3 against oxygen loss.^{18,19} We follow these lines and additionally

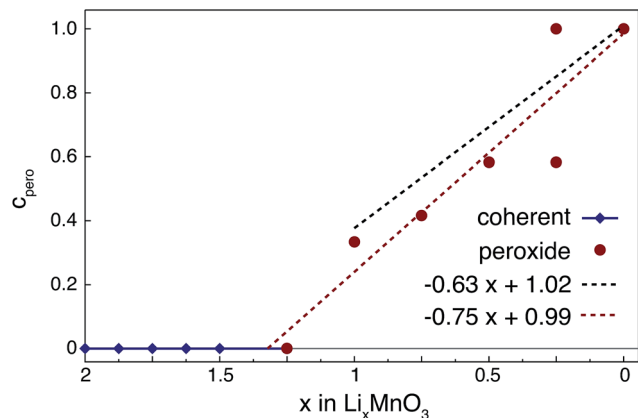


Fig. 7 The most stable concentration of peroxide as a function of the Li concentration in Li_xMnO_3 . The black line is derived from eqn (2) and the red line is a linear regression through the peroxide data.

take into account the peroxide structures by calculation of the reaction energy

$$\Delta H(x) = E(\text{Li}_x\text{MO}_{y-\delta}) - E(\text{Li}_x\text{MO}_y) + \frac{\delta}{2}E(\text{O}_2) \quad (3)$$

where E is the ground state energy per formula unit of the corresponding phases, δ is the concentration of a single oxygen vacancy in our cell, and $E(\text{O}_2)$ includes an over-binding correction as described in ref. 47.

The values in Fig. 8 are classified into phases with a coherent oxygen lattice (blue) and those containing peroxides (red). In agreement with previous findings,¹⁹ the defect-free material is stable at low states of charge, but becomes increasingly prone to spontaneous oxygen release upon delithiation. The peroxide phases, on the other hand, exhibit increasing stability upon delithiation, and while the distorted configurations at intermediate Li concentrations (near $x = 1$) may spontaneously release oxygen, all subsequent ($x < 1$) reaction energies are positive. These results oppose the hypothesis that oxygen dimers form as an intermediate before oxygen release.²⁰ Since we expect oxygen close to the particle's surface to directly react with the electrolyte, this does, however, not contradict the indirectly observed oxygen loss from the material.^{2,4}

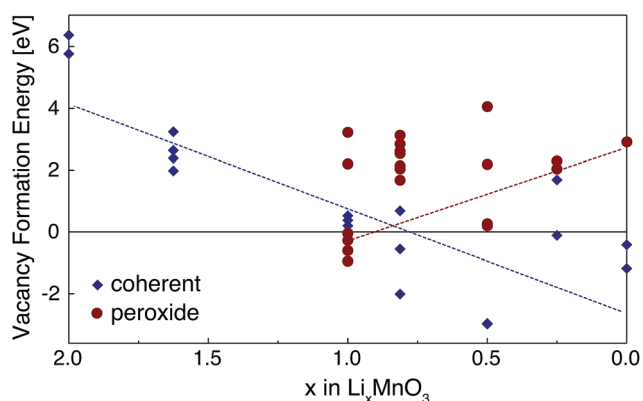


Fig. 8 Oxygen vacancy formation energy as a function of lithiation in Li_xMnO_3 ; the dashed lines are to guide the eye.

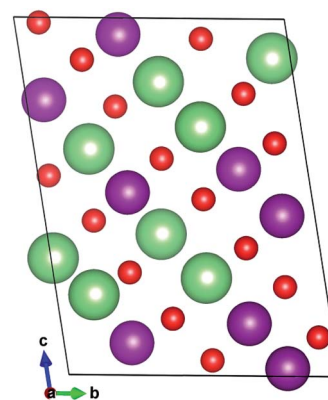


Fig. 9 Lowest energy structure of LiMnO_2 ; found with global optimization of the half-lithiated $\text{LiMnO}_{3-\delta}$ structure with $\delta = 1$, corresponding to eight O vacancies.

The vacancy formation energy is calculated by removal of an O atom. When structures containing both, structural oxygen and peroxides, were considered, vacancies in the peroxide species were most stable because of their low charge and lack of covalency with Mn. The red dashed line in Fig. 8 can therefore be interpreted as the increasing energy required to break up a dimer as Li is removed from the material. It should be noted that the overbinding-correction used is valid for oxides and might be too large for peroxides.⁴⁸ This would then lead to an over-stabilization of the peroxide phases against oxygen loss. Since in the mixed structures removal of an oxygen atom from a peroxide dimer is consistently most favorable, however, a possible over-stabilization of the peroxides does not seem to be an issue.

In view of the driving force for spontaneous oxygen release at half delithiation, oxygen deficient structures have been investigated *via* basin hopping. Upon removal of one third of the anions, giving a ratio of MnO_2 , the geometry densifies to a layered LiMnO_2 phase with cationic disorder (Fig. 9). The decrease in energy of more than 1 eV per FU shows the driving force for the reported mechanism, $\text{Li}_2\text{MnO}_3 - \frac{1}{2}\text{O}_2 - \text{Li} \rightarrow \text{LiMnO}_2$.⁶⁻⁸ An ordered rhombohedral LiMnO_2 version of this phase is found to be even more stable.

Thus, if enough oxygen is released from Li_2MnO_3 , it may transform to LiMnO_2 , which can then take part in charge compensation *via* Mn^{3+} oxidation. Due to the loss of Li sites, such a mechanism would reduce the material capacity; the expected transformation of LiMnO_2 to spinel^{43,49} would also further decrease the voltage. The loss of oxygen necessary for densification, may, however, be kinetically impeded in the bulk¹⁹ and spinel formation may therefore only occur at the particle's surface, as reported in ref. 7. Such model is in agreement with recent works⁵⁰ stating that the release of oxygen and the formation of a spinel-like phase exclusively take place at the particle's surface.

4 Conclusions

Our DFT calculations show that Li_2MnO_3 becomes increasingly unstable upon delithiation and experiences a driving force for

either oxygen release or peroxide formation at less than 50% Li concentration. If oxygen diffusion is kinetically impeded, anion release may primarily occur at the surface and lead to the observed densification to LiMnO_2 and spinel. Peroxide formation is therefore expected to compensate the charge in the bulk while the associated low voltage activity impedes the overall energy density. The observed formation of Mn^{3+} may additionally lead to phase transformations that further reduce the voltage.

Upon relithiation, the symmetric peroxide dimer lattice remains stable up to $\text{Li}_{0.75}\text{MnO}_3$ and experiences a driving force to transform to an ordered phase at much higher Li concentrations. The peroxides formed at high delithiation may therefore transform back into a coherent oxygen lattice at much higher Li concentrations, which explains the observed hysteresis in cycling experiments. The change in energy upon dimerization strongly depends on the concentration of Li and existing peroxide species in the structure. As opposed to the coherent oxygen lattice structure, peroxide dimer phases become increasingly stable with respect to oxygen loss upon delithiation. The material therefore experiences two competing mechanisms at high states of charge: (i) irreversible oxygen release and densification at the surface or (ii) peroxide formation in the bulk. As demonstrated, both are detrimental for the electrochemistry and therefore the stabilization of oxygen is imperative to commercialize over-lithiated transition metal oxides. Based on our results this can only be achieved by elemental substitution in the bulk.

Acknowledgements

This work was supported by the Ruhr University Research School, funded by the Germany Excellence Initiative [DFG GSC 98/3]. The work in Austin was supported by the Welch Foundation under grant F-1841. Computational resources were provided by the Texas Advanced Computing Center. We thank Dr Benedikt Ziebarth for the insightful discussions.

References

- 1 P. Rozier and J.-M. Tarascon, *J. Electrochem. Soc.*, 2015, **162**, A2490–A2499.
- 2 D. Y. Yu, K. Yanagida, Y. Kato and H. Nakamura, *J. Electrochem. Soc.*, 2009, **156**, A417–A424.
- 3 J. R. Croy, M. Balasubramanian, K. G. Gallagher and A. K. Burrell, *Acc. Chem. Res.*, 2015, **48**, 2813–2821.
- 4 S. F. Amalraj, B. Markovsky, D. Sharon, M. Talianker, E. Zinigrad, R. Persky, O. Haik, J. Grinblat, J. Lampert, M. Schulz-Dobrick, A. Garsuch, L. Burlaka and D. Aurbach, *Electrochim. Acta*, 2012, **78**, 32–39.
- 5 S. D. S. D. Pasero, V. McLaren and A. R. West, *Chem. Mater.*, 2005, **17**, 345–348.
- 6 F. Amalraj, M. Talianker, B. Markovsky, D. Sharon, L. Burlaka, G. Shafir, E. Zinigrad, O. Haik, D. Aurbach, J. Lampert, M. Schulz-Dobrick and A. Garsuch, *J. Electrochem. Soc.*, 2013, **160**, A324–A337.
- 7 A. Boulineau, L. Simonin, J. F. Colin, C. Bourbon and S. Patoux, *Nano Lett.*, 2013, **13**, 3857–3863.
- 8 D. Mohanty, S. Kalnaus, R. A. Meisner, K. J. Rhodes, J. Li, E. A. Payzant, D. L. Wood III and C. Daniel, *J. Power Sources*, 2013, **229**, 239–248.
- 9 J. R. Croy, J. S. Park, F. Dogan, C. S. Johnson, B. Key and M. Balasubramanian, *Chem. Mater.*, 2014, **26**, 7091–7098.
- 10 K. Y. Denis and Y. W. Yu, *J. Electrochem. Soc.*, 2011, **158**, A1015–A1022.
- 11 H. Koga, L. Croguennec, M. Menetrier, K. Douhil, S. Belin, L. Bourgeois, E. Suard, F. Weill and C. Delmas, *J. Electrochem. Soc.*, 2013, **160**, A786–A7921.
- 12 H. Koga, L. Croguennec, M. Ménétrier, P. Mannesiez, F. Weill and C. Delmas, *J. Power Sources*, 2013, **236**, 250–258.
- 13 M. Sathiya, K. Ramesha, G. Rousse, D. Foix, D. Gonbeau, A. S. Prakash, M. L. Doublet, K. Hemalatha and J.-M. Tarascon, *Chem. Mater.*, 2013, **25**, 1121–1131.
- 14 M. Sathiya, G. Rousse, K. Ramesha, C. Laisa, H. Vezin, M. Sougrati, M. L. Doublet, D. Foix, D. Gonbeau, W. Walker, A. S. Prakash, M. Ben Hassine, L. Dupont and J.-M. Tarascon, *Nat. Mater.*, 2013, **12**, 827–835.
- 15 E. McCalla, A. M. Abakumov, M. Saubanère, D. Foix, E. J. Berg, G. Rousse, M.-L. Doublet, D. Gonbeau, P. Novák, G. Van Tendeloo, R. Dominko and J.-M. Tarascon, *Science*, 2015, **350**, 1516–1521.
- 16 E. McCalla, M. T. Sougrati, G. Rousse, E. J. Berg, A. Abakumov, N. Recham, K. Ramesha, M. Sathiya, R. Dominko, G. Tendeloo, P. Novak and J.-M. Tarascon, *J. Am. Chem. Soc.*, 2015, **137**, 4804–4814.
- 17 Y. Koyamaa, I. Tanakaa, M. Nagaob and R. Kannob, *J. Power Sources*, 2009, **189**, 798–801.
- 18 R. Xiao, H. Li and L. Chen, *Chem. Mater.*, 2012, **24**, 4242–4251.
- 19 E. Lee and K. A. Persson, *Adv. Energy Mater.*, 2014, **4**, 1400498.
- 20 H. Chen and M. S. Islam, *Chem. Mater.*, 2016, **28**, 18.
- 21 D.-H. Seo, J. Lee, A. Urban, R. Malik, S. Kang and G. Ceder, *Nat. Chem.*, 2016, **8**, 692–697.
- 22 G. Kresse and J. Hafner, *Phys. Rev. B: Condens. Matter Mater. Phys.*, 1993, **47**, 558.
- 23 G. Kresse and J. Hafner, *Phys. Rev. B: Condens. Matter Mater. Phys.*, 1994, **49**, 14251.
- 24 G. Kresse and J. Furthmüller, *Comput. Mater. Sci.*, 1996, **6**, 15.
- 25 J. P. Perdew, K. Burke and M. Ernzerhof, *Phys. Rev. Lett.*, 1996, **77**, 3865–3868.
- 26 J. P. Perdew, K. Burke and M. Ernzerhof, *Phys. Rev. Lett.*, 1997, **78**, 1396.
- 27 P. E. Blöchl, *Phys. Rev. B: Condens. Matter Mater. Phys.*, 1994, **50**, 17953–17979.
- 28 G. Kresse and D. Joubert, *Phys. Rev. B: Condens. Matter Mater. Phys.*, 1999, **59**, 1758–1775.
- 29 P. Xiao, Z. Q. Deng, A. Manthiram and G. Henkelman, *J. Phys. Chem. C*, 2012, **116**, 23201–23204.
- 30 G. Hautier, S. P. Ong, A. Jain, C. J. Moore and G. Ceder, *Phys. Rev. B: Condens. Matter Mater. Phys.*, 2012, **85**, 155208.
- 31 W. Tang, E. Sanville and G. Henkelman, *J. Phys.: Condens. Matter*, 2009, **21**, 084204.

- 32 J. Heyd, G. E. Scuseria and M. Ernzerhof, *J. Chem. Phys.*, 2003, **118**, 8207.
- 33 D. J. Wales and J. P. K. Doye, *J. Phys. Chem. A*, 1997, **101**, 5111–5116.
- 34 D. J. Wales and H. A. Scheraga, *Science*, 1999, **285**, 1368–1372.
- 35 S. R. Bahn and K. W. Jacobsen, *Comput. Sci. Eng.*, 2002, **4**, 56–66.
- 36 M. Koichi and I. Fujio, *J. Appl. Crystallogr.*, 2011, **44**, 1272.
- 37 J. Reed and G. Ceder, *Electrochem. Solid-State Lett.*, 2002, **5**, A145–A148.
- 38 X. Wan, M. Kohno and X. Hu, *Phys. Rev. Lett.*, 2005, **95**, 146602.
- 39 M. Sathiya, J.-B. Leriche, E. Salager, D. Gourier, J.-M. Tarascon and H. Vezin, *Nat. Commun.*, 2015, **6**, 6276.
- 40 Y. Li, M. Bettge, B. Polzin, Y. Zhu, M. Balasubramanian and D. P. Abraham, *J. Electrochem. Soc.*, 2013, **160**, A3006–A3019.
- 41 K. M. Shaju, G. V. Subba Rao and B. V. R. Chowdari, *Electrochem. Commun.*, 2002, **4**, 633–638.
- 42 P. Manikandan, M. V. Ananth, T. P. Kumar, M. Raju, P. Periasamy and K. Manimaran, *J. Power Sources*, 2011, **196**, 10148–10155.
- 43 J. Reed, G. Ceder and A. Van der Ven, *Electrochem. Solid-State Lett.*, 2001, **4**, A78–A81.
- 44 S. Chen and L.-W. Wang, *Phys. Rev. B: Condens. Matter Mater. Phys.*, 2014, **89**, 014109.
- 45 H. Chen and N. Umezawa, *Phys. Rev. B: Condens. Matter Mater. Phys.*, 2014, **90**, 035202.
- 46 J. R. Croy, H. Iddir, K. Gallagher, C. S. Johnson, R. Benedek and M. Balasubramanian, *Phys. Chem. Chem. Phys.*, 2015, **17**, 24382–24391.
- 47 L. Wang, T. Maxisch and G. Ceder, *Phys. Rev. B: Condens. Matter Mater. Phys.*, 2006, **73**, 195107.
- 48 S. Kang, Y. Mo, S. P. Ong and G. Ceder, *Nano Lett.*, 2014, **14**, 1016–1020.
- 49 R. J. Gummow, D. C. Liles and M. M. Thackeray, *Mater. Res. Bull.*, 1993, **28**, 1249–1256.
- 50 B. Strehle, K. Kleiner, R. Jung, F. Chesneau, M. Mendez, H. A. Gasteiger and M. Piana, *J. Electrochem. Soc.*, 2017, **164**, A400–A406.